Journal of Thermal Analysis and Calorimetry, Vol. 80 (2005) 217–223

REACTIONS WITHIN THE SYSTEM, $2SrCO_3$–Fe_2O_3 Part I. CO_2 atmosphere

P. K. Gallagher[1*], *J. P. Sanders*[2], *P. M. Woodward*[3] *and I. N. Lokuhewa*[3]

[1]Emeritus Prof., Depts. of Chemistry and MS&E, The Ohio State University, Columbus, OH, 43210, USA
Adjunct Prof. Depts. of Chemistry and Ceramic and Materials Eng., Clemson University Clemson, SC, 29632, USA
[2]National Brick Research Center, 100 Clemson Research Park., Anderson, SC, 29625, USA
Adjunct Prof. School of Ceramic and Materials Eng., Clemson University
[3]Dept. of Chemistry, The Ohio State University, Columbus, OH, 43210, USA

Simultaneous TG/DSC and high temperature X-ray diffraction studies were performed on the system $SrCO_3$–Fe_2O_3 in an atmosphere of CO_2 from room temperature to 1300°C. $SrCO_3$ decomposes and reacts simultaneously with the Fe_2O_3 beginning around 850°C. A transient iron rich phase is formed initially, which soon diminishes to yield a mixture of perovskite $SrFeO_{3-x}$ and the iron rich phase $Sr_4Fe_6O_{13}$. Upon cooling the perovskite phase predominantly orders into the brownmillerite structure $Sr_2Fe_2O_5$. There does not appear to be a Hedvall effect associated with the first order phase transformation in $SrCO_3$ at 927°C.

Keywords: *simultaneous TG/DSC, solid-state reactivity, X-ray diffraction*

Introduction

The system, $2SrCO_3$–Fe_2O_3 offers several interesting opportunities to study solid-state reactivity.

- There is a wide range of stoichiometry and structural modifications available for the products of the thermal decomposition because of the variability in the valence of iron and the tendency for the perovskite structure to tolerate large concentrations of vacancies and various ordered patterns of these defects [1].
- The decomposition of $SrCO_3$ may be catalyzed by the presence of Fe_2O_3 [2].
- The decomposition of $SrCO_3$ is reversible and depends upon the partial pressure of CO_2 [3].
- There is the possibility of a 'Hedvall effect', because of the crystallographic transformation in $SrCO_3$ within the temperature range of the reactions [4].

Consequently, the nature and rates of the reactions are investigated as a function of the partial pressures of O_2 and CO_2 using simultaneous TG/DSC and variable temperature X-ray powder diffraction.

When the Sr/Fe ratio is unity the most important ternary phases are the cubic perovskite phase, $SrFeO_{3-x}$, and the orthorhombic brownmillerite phase, $Sr_2Fe_2O_5$. In the presence of significant amounts of O_2 the perovskite phase $SrFeO_{3-x}$ is formed as shown in Eq. (1). In the absence of oxygen vacancies (x=0) the perovskite structure stabilizes the unusual oxidation state of +4 for iron [5]. However, high partial pressures of O_2 are needed to prepare defect free $SrFeO_3$. It has been shown that for samples that are slow cooled the defect concentration at room temperature is $0.09 \geq x \geq 0.12$ when prepared in pure oxygen, $0.20 \geq x \geq 0.16$ when prepared in air, and 0.43 when prepared in an atmosphere with p_{O_2}=0.003 atm [6]. The brownmillerite structure can be derived from the perovskite structure by the ordering of oxygen vacancies in a pattern that leads to distorted tetrahedral coordination for 50% of the iron sites and distorted octahedral coordination for the remaining iron sites [7]. As the temperature is increased, the conditions become more reducing and further oxygen vacancies are created, i.e., the value of x increases. As the value of x approaches 0.5 and the oxidation state of iron approaches +3, the perovskite structure is no longer stable and the brownmillerite structure forms as shown in Eq. (2). Temperature also affects the competition between brownmillerite and perovskite in a direct manner. If brownmillerite, $Sr_2Fe_2O_5$, is heated in an inert atmosphere so that iron remains in the +3 oxidation state over the entire temperature range, the oxygen ion mobility increases with temperature. Eventually the oxygen vacancies become disordered and orthorhombic $Sr_2Fe_2O_5$ brownmillerite transforms to cubic $SrFeO_{2.5}$ defect perovskite. Campbell and Schmidt have shown this to occur at 875°C in an inert atmosphere [8]. In principle, in the absence of available O_2 the brownmillerite phase can be formed directly from $SrCO_3$ and Fe_2O_3 (Eq. (3)).

$$2SrCO_3+Fe_2O_3+(0.5-x)O_2 \leftrightarrow 2SrFeO_{3-x}+2CO_2 \quad (1)$$

$$2SrFeO_{3-x} \leftrightarrow Sr_2Fe_2O_5+(0.5-x)O_2 \quad (2)$$

* Author for correspondence: p_gallag@bellsouth.net

1388–6150/$20.00

Akadémiai Kiadó, Budapest, Hungary
Springer, Dordrecht, The Netherlands

$$2SrCO_3+Fe_2O_3 \leftrightarrow Sr_2Fe_2O_5+2CO_2 \quad (3)$$

Part I of this study concentrates on the decomposition and subsequent reactions in a CO_2 atmosphere. Part II will deal with the effects of oxidation by comparing the results in O_2 and Ar atmospheres.

Experimental

The sources of $SrCO_3$ and Fe_2O_3 were Aldrich (99.995% purity) and Alfa Aesar (Puratronic Grade, 99.998% purity), respectively. The sample was prepared by thoroughly mixing the two materials in the molar proportion of $2SrCO_3$ with Fe_2O_3, i.e. Sr/Fe equals unity, in methanol using a mortar and pestle. After mixing, the methanol was ignited and the resultant mixture was dried at 110°C for 24 h and then stored in a desiccator prior to use.

Simultaneous thermogravimetric/differential scanning calorimetry (TG/DSC) measurements were performed on a Netzsch 449C simultaneous thermal analyzer using open alumina crucibles. The nominal sample size used in this work was 20.3 mg (±0.3 mg). A flowing atmosphere at 100 mL min^{-1} was used for all measurements. The three atmospheres used were Ar, O_2, and CO_2. Nominal heating rates of 1, 2, 4, 8, 16 and 32 K min^{-1} were used in this study. Baselines and sensitivity calibrations were obtained for each heating rate. An empty alumina crucible was used as the reference for the DSC measurements. The sensitivity calibration calculations for the DSC measurements were made using measurements on sapphire disks.

Data analysis was performed using Netzsch's Proteus and Thermokinetic 2 software packages [9]. In the least squares fitting of the TG data no weighing factors were applied. For the TG data set, single step linear regression was performed as well as multi-step non-linear regression analysis using consecutive reactions. Kinetic analysis was not performed on the DSC curves because of the complications due to the multiple phase transformations.

Variable temperature X-ray powder diffraction (XRPD) data sets were collected with a Bruker D8 diffractometer. The diffractometer is equipped with an incident beam Ge 111 monochromator that selects only $CuK_{\alpha 1}$ radiation, a Braun linear position sensitive detector, and an Anton Parr HTK 1200 high temperature stage. The HTK 1200 temperature stage employs ambient heating to minimize temperature gradients. At each temperature the data collection time was 45–60 min before ramping to the next temperature and holding for the next run. The data were collected in flowing atmospheres of Ar, O_2 and CO_2. The data were analyzed using the Rietveld method [10], as implemented in the TOPAS software package [11].

Results and discussion

The effect of CO_2 on the reversible decomposition is indicated in Fig. 1 which presents TG curves, collected at 8 K min^{-1}, for the reactions in O_2, Ar and CO_2. Clearly the reversible decomposition and simultaneous reaction of $SrCO_3$ is shifted about 200°C to higher temperatures in CO_2. This has the effect of essentially separating the phase transformation in $SrCO_3$, around 927°C, from the subsequent reactions. The decomposition and simultaneous reactions, however, are clearly influenced by higher temperature transitions of the reactants and/or products in the case of CO_2. The onset of the decomposition for the mixture is at a slightly lower temperature than for pure $SrCO_3$ itself. The overall mass loss in O_2 is slightly less by virtue of its greater oxidation strength and consequently higher average valence for the iron species. The theoretical mass loss for Eq. (1) with x=0 is 15.83%, for Eq. (2) is 3.52%, and for Eq. (3) is 19.35%.

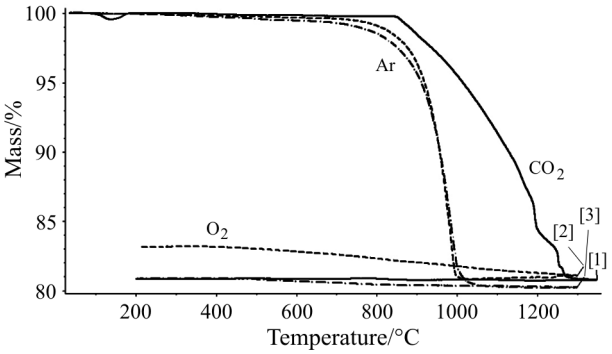

Fig. 1 TG data for $2SrCO_3 \cdot Fe_2O_3$ mixture in O_2, Ar and CO_2 at 8 K min^{-1}

DSC results of the simultaneous TG/DSC experiments in CO_2 at various heating rates are presented in Figs 2 and 3. Figure 2 shows the DSC curves during heating and those during cooling are shown in Fig. 3. The TG curves are seen later in the discussion of the kinetic analyses. Table 1 summarizes the extensive X-ray diffraction study indicating the mass fractions of each solid phase as a function of temperature, and the overall Sr:Fe ratio that would result from such a mixture. As no constraints were placed on the phase fractions during analysis of the X-ray data the deviation of the Sr:Fe ratio from unity acts as an independent indicator of the accuracy of the results. The differences between the time–temperature programs applied to the thermoanalytical and X-ray diffraction experiments preclude a direct comparison. Nevertheless, valuable insights can be obtained through a judicious comparison between the two sets of results.

The general nature of the overall sequence of reactions is described using the intermediate heating rate of 8 K min^{-1} as an example. Figures 4 and 5 show ex-

Table 1 Change in mass% on cooling and heating as determined by Rietveld analysis of the X-ray powder diffraction data[a]

T/°C	$SrCO_3$ Pmcn	$SrCO_3$ R$\bar{3}$m	Fe_2O_3 R$\bar{3}$c	$SrFeO_{3-x}$ Pm$\bar{3}$m	$Sr_4Fe_6O_{13}$ Icc2$_1$	$Sr_4Fe_{2.6}O_{8.2}(CO_3)_{0.4}$ 14/mmm	$SrFe_{12}O_{19}$ P6$_3$/mmc	$Sr_2Fe_2O_5$ Ibm2	Mole ratio Sr/Fe
25	66(3)		34(2)						1.03
800	66(1)		34(1)						1.04
850	63(2)		14(1)		5(0.5)		17(1)		1.13
900	45(1)	7(0.4)	8(0.1)	3(0.4)	18(1)		18(1)		0.97
925		43(1)	3(0.5)	8(0.4)	22(1)		24(1)		0.93
950		38(1)		13(1)	25(1)		23(1)		0.93
975		34(1)		20(1)	25(1)		21(1)		0.91
1000		28(1)		25(1)	30(1)		18(1)		0.88
1025		24(1)		32(1)	33(1)		11(1)		0.94
1050		19(1)		32(1)	34(1)		14(1)		0.87
1075		15(1)		38(1)	37(1)		10(1)		0.84
1100		12(1)		42(1)	40(1)		7(0.9)		0.86
1125		9(0.5)		46(1)	40(1)	6(1)			0.97
1150		5(0.4)		45(1)	43(1)	8(1)			0.91
1150		4(0.6)		47(2)	42(1)	7(1)			0.91
1150		3(0.5)		48(1)	41(1)	8(1)			0.90
1150		3(0.3)		49(2)	40(1)	8(1)			0.90
1150		1(0.4)		52(2)	38(1)	8(1)			0.89
1150		2(0.3)		52(2)	39(1)	7(1)			0.89
1100		1(0.4)		55(2)	38(1)	6(1)			0.88
1050		1(0.4)		54(2)	38(1)	7(1)			0.89
1000		1(0.4)		54(2)	37(1)	8(1)			0.89
950		2(0.4)		60(2)	37(1)				0.88
900		5(0.5)		60(2)	36(1)				0.91
850		5(0.5)		61(2)	36(1)				0.91
800	5(0.8)	2(0.5)		58(2)	34(1)				0.95
750	9(0.08)			59(2)	32(1)				0.95
700	9(0.8)			59(2)	32(1)				0.98
650	6(0.6)			46(2)	31(1)			17(1)	0.95
600	8(0.7)			37(1)	30(1)			25(1)	0.97
550	7(0.7)			32(1)	29(1)			32(1)	0.97
500	8(0.7)			28(1)	28(1)			37(1)	0.98
300	10(1)			21(1)	28(1)			32(1)	1.00
25	8(0.8)			16(1)	25(1)			51(2)	0.99

[a]Estimated standard deviations are enclosed in parentheses.

panded sections of the DTG and DSC curves for the heating and cooling portions, respectively. At about 838°C there are small irregularities noted during heating in the DTG and DSC curves. These are believed to be associated with the very initial onset of the reaction or with an as yet unknown event occurring in $SrCO_3$ which has been observed previously and is the subject of further work [3]. The first order orthorhombic to rhombohedral phase transformation is clearly evident as a relatively sharp endothermic peak in the DSC curve having an extrapolated onset temperature of 927.1°C at this heating rate. The X-ray results in Table 1 confirm the transition. There is no detectable change in either the TG or DTG curves, ruling out any significant enhancement of the rate of the reaction as a result of the phase transformation, i.e., 'Hedvall effect'.

The XRPD results shown in Table 1 provide valuable information about the details of this reaction. At 850°C ternary reaction products begin to appear. This corresponds rather closely with the first sign of

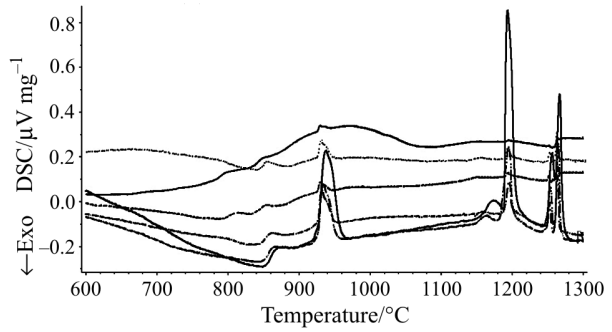

Fig. 2 DSC curves for $2SrCO_3{\cdot}Fe_2O_3$ mixture on heating in CO_2

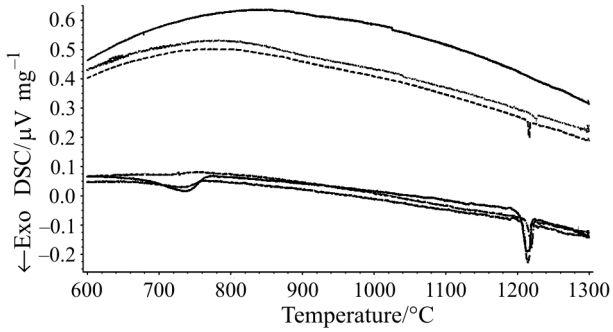

Fig. 3 DSC curves for $2SrCO_3{\cdot}Fe_2O_3$ mixture on cooling in CO_2

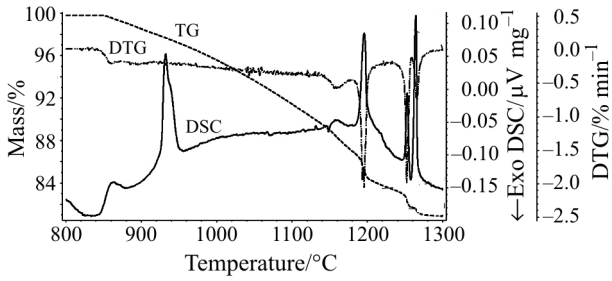

Fig. 4 TG, DTG and DSC curves for $2SrCO_3{\cdot}Fe_2O_3$ mixture on heating in CO_2 at 8 K min^{-1}

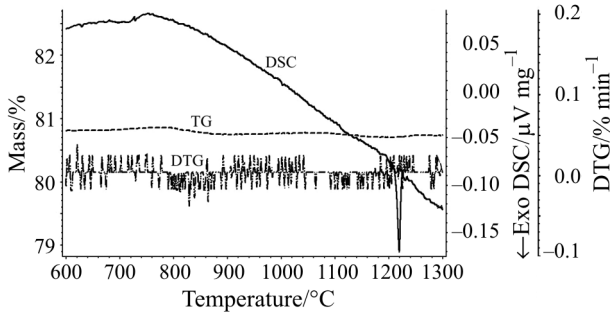

Fig. 5 TG, DTG and DSC curves for $2SrCO_3{\cdot}Fe_2O_3$ mixture on cooling in CO_2 at 8 K min^{-1}

mass loss in the TG data and the small features in the DTG and DSC curves noted above. The simultaneous decomposition of $SrCO_3$ and reaction with Fe_2O_3 is substantiated by the failure to detect SrO in the X-ray patterns. This is in contrast to XRPD patterns collected in argon where SrO formation was clearly seen, as will be discussed in detail in part II. The beginnings of the transformation of $SrCO_3$ from orthorhombic to rhombohedral is first seen in the XRPD data set collected at 900°C and the transformation appears complete at 925°C in reasonably good agreement with the DSC analysis.

The first ternary phases to form are the Fe-rich phases $SrFe_{12}O_{19}$ and $Sr_4Fe_6O_{13}$. The former compound has the magnetoplumbite structure with hexagonal symmetry and structurally related to Fe_2O_3, while the latter phase has a complex orthorhombic structure that is related to perovskite. The concentration of $SrFe_{12}O_{19}$ rises sharply as the $SrCO_3$ and Fe_2O_3 begin to react and then decreases with further heating, disappearing upon heating above 1100°C. The transient appearance of this phase is most likely a result of diffusion limited interfacial reactions. The concentration of $Sr_4Fe_6O_{13}$ climbs to a mass fraction of roughly 40% and then decreases very slowly upon cooling, finally coming to a value of 25 mass% upon cooling all the way back to room temperature. Apparently once this phase forms its decomposition is very sluggish. Thus it acts as a kinetic trap that must be overcome in order to prepare either cubic perovskite or brownmillerite. Significant concentrations of this phase were also observed in air and argon atmospheres, but in air the concentration of this phase decreased more rapidly upon cooling. Apparently $Sr_4Fe_6O_{13}$ does not easily accommodate additional oxygen that must accompany oxidation of iron, and conditions that favor Fe^{4+} are needed in order to stabilize the cubic perovskite phase in preference to $Sr_4Fe_6O_{13}$. A recent study of phase equilibria in the SrO–Fe_2O_3 system shows that in the temperature range 800–1200°C an equilibrium mixture of $SrFeO_3$ and $Sr_4Fe_6O_{13}$ is expected when the Fe:Sr ratio is between 1.0 and 1.5 [12]. Therefore, given the presence of unreacted $SrCO_3$ and the Sr-rich oxycarbonate phase $Sr_4Fe_{2.6}O_{8.2}(CO_3)_{0.4}$ the presence of $Sr_4Fe_6O_{13}$ is to be expected. The existence of both of these phases is based on the appearance a few weaks peaks in the X-ray patterns. Consequently, it is difficult to accurately determine their phase fractions.

The presence of an oxycarbonate phase, $Sr_4Fe_{2.6}O_{8.2}(CO_3)_{0.4}$, at high temperature was not anticipated in advance, nor could it have been anticipated from the thermal analysis data. The structure of this phase is closely related to the Ruddlesden–Popper (RP) series of compounds, in particular $Sr_4Fe_3O_{10}$ [13]. In order to confirm and better understand the formation of this phase the RP phase $Sr_3Fe_2O_{7-x}$ was pre-

pared and its stability was studied in a CO_2 atmosphere by variable temperature X-ray diffraction. Upon heating above 700°C the RP starts to decompose to form $SrCO_3$ and $SrFeO_{3-x}$. Upon heating above 1100°C the oxycarbonate phase forms. This phase appears only to be stable at high temperatures because on cooling below 1000°C it decomposes to form $SrCO_3$ and $SrFeO_{3-x}$. These temperatures are in good agreement with the temperature range where the oxycarbonate phase is observed in Table 1. From this behavior we can also infer that the increase in the quantity of $SrCO_3$ that is seen in Table 1 upon cooling can be attributed to the decomposition of the oxycarbonate phase. The TG data suggests that if the X-ray furnace could access higher temperatures both the oxycarbonate and the $SrCO_3$ phases would have decomposed and reacted with the iron rich $Sr_4Fe_6O_{13}$ phase to form pure $SrFeO_{3-x}$ perovskite.

At the highest temperatures the dominant phases are $Sr_4Fe_6O_{13}$ and the cubic perovskite phase, $SrFeO_{3-x}$. While it may initially seem surprising to form cubic perovskite instead of $Sr_2Fe_2O_5$ brownmillerite at high temperature in a CO_2 atmosphere, bear in mind that the cubic perovskite structure can support considerable oxygen non-stoichiometry at high temperature. As stated in the introduction pure $Sr_2Fe_2O_5$ has been shown to undergo a phase transition from the orthorhombic brownmillerite structure to an oxygen deficient cubic perovskite structure upon heating above 875°C in an argon atmosphere [8]. At high temperature in a CO_2 atmosphere the oxidation state of iron should be close to +3, and order–disorder transition should occur at a similar temperature. Schmidt and Campbell found the lattice parameter of the disordered cubic form of $Sr_2Fe_2O_5$ ($SrFeO_{2.5}$) to vary from 3.976 Å at 875°C to 3.982 Å at 950°C in argon [8, 14]. They also studied $SrFeO_{2.81}$ upon heating in air and found that at 1000°C the cubic perovskite phase had a composition of $SrFeO_{2.56}$ and a unit cell parameter of 3.985 Å. By comparison the unit cell parameter for the cubic perovskite phase in this experiment was determined to be 3.9792(3) Å at 950°C upon cooling. Therefore, it can be concluded that the stoichiometry of the high temperature cubic perovskite phase seen in the XRPD patterns is fairly close to $SrFeO_{2.5}$. The pre-dominance of Fe in the +3 oxidation state in both the cubic perovskite and the $Sr_4Fe_6O_{13}$ phases is consistent with the TG results.

Upon cooling below 850°C the cubic perovskite phase starts transforming back into the orthorhombic brownmillerite phase as the oxygen vacancies order. Surprisingly, roughly 16% of the cubic perovskite phase was retained upon cooling back to room temperature. The lattice parameter of the cubic phase that remains at room temperature, 3.8948(9) Å, is quite close to the value of 3.894 Å reported for $SrFeO_{2.81}$ at 300°C [14]. From this observation it is concluded that some oxidation occurred in the high temperature X-ray stage that prevented complete transformation to brownmillerite upon cooling. We suspect adventitious oxygen that was not completely flushed from the system.

The decomposition and reactions proceed until completion around 1280°C. There are four general areas of enhanced rate particularly evident in the DTG curve peaking at 1160, 1196, 1253 and 1259°C. There are obvious endotherms in the DSC curve associated with them. Unfortunately all are right at or above the upper temperature limit of the X-ray diffraction study. These are attributed to unknown $solid_1$, $solid_2$ or solid–liquid phase transformations.

The thermoanalytical curves on cooling, Fig. 5 show less features, as would be expected. There is a prominent sharp exotherm, presumably resulting from solidification of the highest temperature melt. There is a change of slope, and perhaps a small peak (depending on one's choice of baseline, around 750°C consistent with oxygen vacancy ordering in $Sr_2Fe_2O_5$ observed in the X-ray study. The TG results show no significant gain in mass upon cooling in CO_2 implying no re-carbonation during cooling.

Earlier work had indicated superior results were achieved using the TG rather than the DSC data for kinetic analysis of simultaneous TG/DSC results [15]. In addition, the multiple phase transformations obvious in Fig. 3 would invalidate such a DSC based analysis. The TG data were analyzed using two approaches. Only the data below a fraction reacted, α, of 0.7 was used because of the irregularities imposed by the melting at high temperatures.

The traditional kinetic analyses of thermoanalytical data has justifiably been the subject of much criticism in recent times, e.g., the extensive review by Galwey [16]. The analyses herein are an attempt to access the utilization of conventional commercial programming to gain insights into an obviously very complex reaction system. Recognizing that such analyses represent a compromise between achieving the best fit and minimizing the number of variable parameters, a single step mechanism was used initially [15]. Model-free kinetic analysis using the Ozawa–Flynn analysis was applied first. Figure 6 summarizes the results. In the region $0.2<\alpha<0.6$ the Arrhenius parameters are reasonably constant. A value of about 500 kJ mol^{-1} is obtained for the apparent activation energy, E, and about 16 for the log of the corresponding pre-exponential term, $\log A$. At either extreme of α, the values rise abruptly and, as usual, an apparent correlation effect is observed between E and $\log A$.

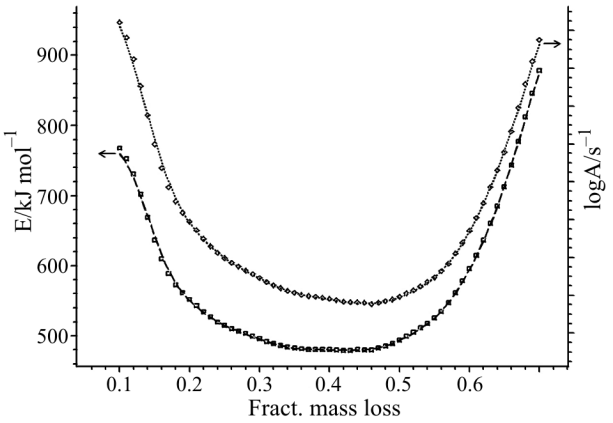

Fig. 6 Ozawa–Flynn model-free analysis of TG data for $2SrCO_3{\cdot}Fe_2O_3$ mixture (heating in CO_2), α=0.1 to 0.7

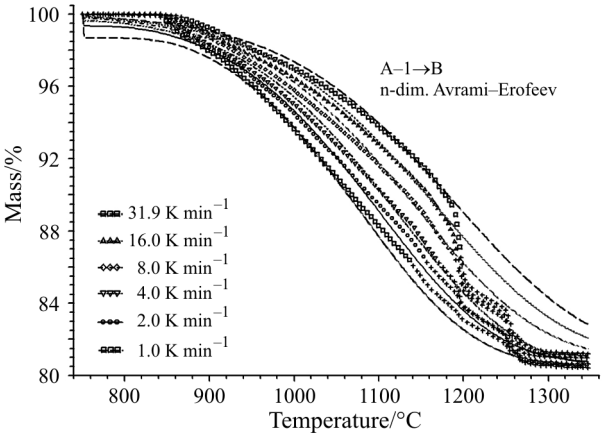

Fig. 7 Single step data fit of TG data for $2SrCO_3{\cdot}Fe_2O_3$ mixture (heating in CO_2), α=0.1 to 0.7

Allowing the kinetics software package to achieve the best fit by single step linear regression produced the result summarized in Table 2. Figure 7 indicates the fit to the experimental data. The Arrhenius parameters from the Avrami–Erofeev mechanism are in fair agreement with those suggested by the Ozawa–Flynn analysis.

In Figs 1 and 4, however, it is obvious the first several mass percent of the reaction appear to have a significantly different reaction rate. Consequently, it is reasonable to introduce a two-step process into the analysis. The optimum results using a two-step consecutive reaction mechanism are summarized in Table 3. The much improved fit is illustrated in Fig. 8. The Avrami–Erofeev is still the mechanism of choice for the major portion of the reaction, above α=0.16 and the Arrhenius parameters are very similar to those for the single-step process. An n^{th} order reaction, however, is selected for the first portion of the reaction. The Arrhenius parameters derived and the order of this step are unreasonably high, however.

Table 2 Kinetic parameters for single step kinetic modeling

Model type	Avrami–Erofeev
fit range/α	0.1–0.7
log$A$/s^{-1}	15
E/kJ mol^{-1}	478
reaction dimension	0.27
R^2	0.996

Table 3 Kinetic parameters for multi-step kinetic modeling

Model type	First step	Second step
	n^{th} order	Avrami–Erofeev
fit range/α	0.1–0.7	
log$A$/s^{-1}	56	14
E/kJ mol^{-1}	1276	444
reaction order	21	
reaction dimension		0.32
following reaction	0.16	
R^2	0.999	

The two-step process invoking a change in mechanism after about 16% of the decomposition correlates well with the observation of the transient phase, $SrFe_{12}O_{19}$. It is proposed that the initial rate corresponds to the formation of the transient phase and then transforms to that primarily associated with the formation of the final products. An alternative explanation invokes the first order phase transformation of $SrCO_3$. The change in mechanism appears very close to the transition temperature. This suggests that, although no momentary enhancement of the rate is associated with the transition, there may be a significant difference in the rate and/or mechanism occurring between the two crystallographic phases.

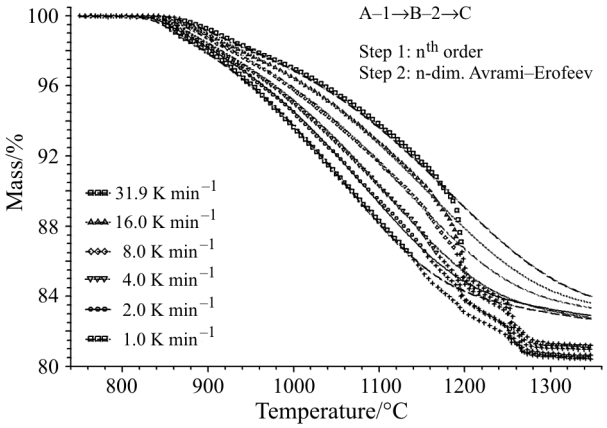

Fig. 8 Multi-step data fit of TG data for $2SrCO_3{\cdot}Fe_2O_3$ mixture (heating in CO_2), α=0.1 to 0.7

Conclusions

- Because of the reversible nature of the thermal decomposition of $SrCO_3$, the decomposition and simultaneous reaction with Fe_2O_3 does not begin until approximately 850°C.
- Initially the iron rich phases, $SrFe_{12}O_{19}$ and $Sr_4Fe_6O_{13}$ are formed followed closely by the cubic perovskite $SrFeO_{3-x}$. While $SrFe_{12}O_{19}$ is a transient phase that decomposes on further heating, $Sr_4Fe_6O_{13}$ does not decompose easily once it is formed. Above 1100°C the oxycarbonate phase $Sr_4Fe_{2.6}O_{8.2}(CO_3)_{0.4}$ forms. There are indications of melting and further reaction in the DSC curves above about 1150°C.
- Upon cooling below 1000°C the oxycarbonate phase decomposes to form $SrFeO_{3-x}$ and $SrCO_3$. Upon cooling somewhere in the vicinity of 700–750°C the oxygen vacancies in the cubic perovskite phase ($SrFeO_{2.5}$) order and a transformation to the orthorhombic brownmillerite phase ($Sr_2Fe_2O_5$) is observed.
- There does not appear an obvious enhancement in the reaction rate, Hedvall effect, associated with first order phase transformation in $SrCO_3$ at 927°C, even at the slowest heating rates.
- Utilizing traditional software, the reaction appears best modeled using TG data with a two-step process involving an initial nth order reaction followed by an Avrami–Erofeev type reaction after an α of about 0.16. Only data below α=0.7 were fit because the higher temperature reactions markedly influenced the rate of mass loss. DSC data were not analyzed kinetically because of these complications. Little faith, however, can be placed in the direct implications of these simplified analyses. This in no way reflects on the software used but is the result of the underlying assumptions inherent in traditional kinetic analysis and the complexity of the reactions.
- A two-step mechanism could be supported either by the formation of the transient iron rich intermediate at the heating rates used or by a difference in reactivity of the two crystallographic forms of the reactant $SrCO_3$.

References

1 P. K. Gallagher, in Application of Mössbauer Spectroscopy, R. L. Cohen (Ed.), Academic Press, New York 1976, Chap. 7 and references therein.
2 P. K. Gallagher and D. W. Johnson, Jr., J. Am. Cer. Soc., 59 (1976) 171.
3 S. A. Robbins, R. G. Rupard, B. J. Weddle, T. R. Maull and P. K. Gallagher, Thermochim. Acta, 269/270 (1995) 43.
4 J. A. Hedvall, Chem. Rev., 15 (1934) 139.
5 P. K. Gallagher, J. B. MacChesney and D. N. E. Buchanan, J. Chem. Phys., 41 (1964) 2429.
6 M. Schmidt, J. Phys. Chem. Solids, 61 (2000) 1363.
7 R. H. Mitchell, 'Perovskites: Modern and Ancient' Almaz Press, Thunder Bay, Ontario, Canada 2002.
8 M. Schmidt and S. J. Cambell, J. Solid State Chem., 156 (2001) 292.
9 J. Opffermann, J. Therm. Anal. Cal., 60 (2000) 641.
10 R. A. Young, 'The Rietveld Method' Oxford University Press, London 1995, Chap. 1.
11 R. W. Cheary and A. A. Coelho, J. Appl. Cryst., 25 (1992) 109.
12 A. Fossdal, M. A. Einarsrud and R. Grande, J. Solid State Chem., 177 (2004) 2933.
13 Y. Bréard, C. Michel, M. Hervieu and B. Raveau, J. Mater. Chem., 10 (2000) 1043.
14 M. Schmidt and S. J. Cambell, J. Phys. Chem. Solids, 63 (2002) 2085.
15 J. P. Sanders and P. K. Gallagher, Thermochim. Acta, 388 (2002) 115.
16 A. K. Galwey, Thermochim. Acta, 423 (2004) 139.